RSC Advances

PAPER

View Article Online
View Journal | View Issue

Cite this: *RSC Adv.*, 2023, **13**, 6656

Vitrimer ionogels towards sustainable solid-state electrolytes†

Fengdi Li, Giao T. M. Nguyen, Cédric Vancaeyzeele, Frédéric Vidal and Cédric Plesse*

The growing demand for flexible, stretchable, and wearable devices has boosted the development of ionogels used as polymer electrolytes. Developing healable ionogels based on vitrimer chemistry is a promising approach to improve their lifetimes as these materials are usually subjected to repeated deformation during functioning and are susceptible to damage. In this work, we reported in the first place the preparation of polythioether vitrimer networks based on the not extensively studied associative *S*-transalkylation exchange reaction using thiol–ene Michael addition. Thanks to the exchange reaction of sulfonium salts with thioether nucleophiles, these materials demonstrated vitrimer properties such as healing and stress relaxation. The fabrication of dynamic polythioether ionogels was then demonstrated by loading 1-ethyl-3-methylimidazolium bis(trifluoromethylsulfonyl)imide or 1-ethyl-3-methylimidazolium trifluoromethanesulfonate (EMIM triflate) within the polymer network. The resulting ionogels exhibited Young's modulus of 0.9 MPa and ionic conductivities in the order of 10^{-4} S cm^{-1} at room temperature. It has been found that adding ionic liquids (ILs) changes the dynamic properties of the systems, most likely due to a dilution effect of the dynamic functions by the IL but also due to a screening effect of the alkyl sulfonium OBrs-couple by the ions of the IL itself. To the best of our knowledge, these are the first vitrimer ionogels based on an *S*-transalkylation exchange reaction. While the addition of ILs resulted in less efficient dynamic healing at a given temperature, these ionogels can provide materials with more dimensional stability at application temperatures and can potentially pave the way for the development of tunable dynamic ionogels for flexible electronics with a longer lifespan.

Received 29th October 2022
Accepted 20th February 2023

DOI: 10.1039/d2ra06829j

rsc.li/rsc-advances

Introduction

The growing demand for flexible, stretchable, and wearable electronic devices has emphasized a need for stretchable electronic and ionically conducting materials. Among these materials, the recent development in ionically conducting materials has boosted the development of electrochemical devices (*e.g.*, batteries and fuel cells, supercapacitors, electrochromic devices) and has opened the door to flexible and wearable sensors, intronics, *etc.*[1–8] These ionically conducting materials are gel-like materials that make it possible to combine the mechanical properties of the polymer network with the ionic conductivity of the liquid electrolyte.[3] Depending on the nature of the liquid phase, different types of gels are described: hydrogels (salt + water), organogels (salt + organic solvent), or more recently ionogels (ionic liquid).[9] Ionogels are termed as a class of ionically conducting materials when the ionic liquid (IL) is percolated through a polymer network. Such materials are more precisely achieved by *in situ* gel network formation in an IL or by swelling a polymer gel network with ILs.[1,2] Ionogels combine the mechanical properties of the crosslinked polymer networks with the ionic conductivity, non-volatility and non-flammability of ILs.[1,2,7–9]

In the frame of their applications and especially in the rising field of flexible, stretchable, and wearable devices, ionogels are usually subjected to repeated deformation during functioning, making them susceptible to damage. Thus, developing a simple and effective approach to improve their durability and life span becomes crucial. Imparting ionogels with self-healing ability seems likely a promising strategy because of their capabilities to repair mechanically induced damages. Healable ionogels based on hydrogen bonds, ionic bonds or metal–ligand coordination have been widely studied.[10–13] Despite that ionic and hydrogen bonds are known to achieve efficient self-healing performances, these are generally strongly impacted by heat, the presence of water and any other polar solvents, which might be limiting in regard to their practical applications. Another strategy to impart materials with healing functionality is to introduce reversible reactions including covalent bonds. Fabrication of dynamic reversible polymer networks has become a popular strategy, particularly by introducing exchangeable chemical bonds into

Laboratory of Physicochemistry of Polymers and Interfaces, CY Cergy Paris University, 5 Mail Gay Lussac, 95000 Neuville sur Oise, France. E-mail: cedric.plesse@cyu.fr

† Electronic supplementary information (ESI) available: Experiments discussed here including ^{1}H NMR spectra, and characterizations by DSC and rheometer. See DOI: https://doi.org/10.1039/d2ra06829j

polymer networks, which are known as covalent adaptable networks (CANs). Based on the intrinsic mechanism of bond exchange reaction, CANs are further divided into dissociative and associative mechanisms.[14] In dissociative CANs, bonds are first broken and then reformed in response to external stimuli, such as heat or light.[14–16] Such dissociative bond exchange reactions have been used to prepare healable ionogels. For example, ionogels composed of chemically crosslinked poly(furfuryl methacrylate-*co*-methyl methacrylate) (P(FMA-*co*-MMA)) and physically crosslinked poly(vinylidene fluoride-*co*-hexafluoropropylene) (P(VDF-*co*-HFP)) networks with 80 wt% of 1-ethyl-3-methylimidazolium bis(trifluoromethylsulfonyl) imide (EMIM TFSI) loading have been prepared.[17] The furan-maleimide crosslinker used in the network endowed the ionogel with a fast thermal healing efficiency thanks to the dissociative reversible Diels–Alder exchange reaction while the IL content provided the material with an ionic conductivity of 3.3 mS cm^{-1} at room temperature. Li *et al.* designed ionic skins by impregnating 1,2-dimethyl-3-ethoxyethylimidazolium bis(trifluoromethanesulfonyl)imide (DEIM TFSI) into a mechanically robust poly(urea-urethane) network with an ionic conductivity of 1.2 mS cm^{-1}.[18] The dissociative dynamic hindered urea bonds and hydrogen bonds between the amide groups endowed ionogel with healing ability. However, dissociative CANs allow topology rearrangements due to uncrosslinking of the material associated with a sudden drop of viscosity. This feature is a drawback in applications that require dimensional stability, easy shaping, and welding process. On the contrary, CANs that rely on an associative bond exchange reaction are characterized by a constant crosslink density.[19] The bond cleavage is accompanied by the simultaneous formation of a new crosslink, as a result, such systems can change their topology with no loss of connectivity, making such networks permanent and insoluble. More specifically, in 2011, the term 'vitrimers' was introduced by Leibler *et al.* for thermally triggered associative CANs.[20] Some groups reported vitrimer ionogels. Healable and reprocessable gelatin ionogels based on reversible exchange of imine bonds have been designed for flexible supercapacitors.[21] These dynamic ionogels demonstrated an ionic conductivity higher than 1 mS cm^{-1} at room temperature thanks to the use of 1-ethyl-3-methylimidazolium acetate (EMIM Ac). Xu *et al.* reported polyurethane (PU) ionogels demonstrating an ionic conductivity of about 14 mS cm^{-1}.[22] The cracked PU ionogels can be readily healed at room temperature and restore their original performance owing to the dynamic boronic ester crosslinker used in the polymer network. Another team also showcased healable and recyclable boronic ester-based ionogels using 1-butyl-3-methylimidazolium tetrafluoro-borate. However, imine bonds and boronic ester are sensitive to water and can undergo dissociative hydrolysis, which impacts the stability of the materials and limit their applications.[23]

Recently, Zhong *et al.* reported polythioether (PTE)/EMIM TFSI ionogels with tailorable surface and mechanical properties using thiol–ene Michael addition.[1,2] The nearly ideal 1 : 1 stoichiometric reactivity of thiol–ene Michael addition enabled fine-tuning of surface and mechanical properties of ionogels. While these materials are initially permanent and non-dynamic networks, Hendriks *et al.* reported turning PTE networks into catalyst-free vitrimer networks by covalently incorporating an alkylation agent (butyl brosylate BuOBrs) through thermal treatment.[24] The resulting poly(thioether-sulfonium) materials can be recycled and remolded without loss of mechanical properties at elevated temperature through the *S*-transalkylation reaction of sulfonium salts with thioether nucleophiles. Moreover, this exchange reaction is not water sensitive. Combining tailorable PTE/EMIM TFSI ionogels with *S*-transalkylation seems very promising to develop healable ionogels based on associative dynamic covalent bonds.

Herein, *S*-transalkylation polythioether networks were first prepared to study the dynamic properties of this not extensively studied chemistry. These networks were prepared through the thiol–ene Michael addition between multifunctional thiols and diacrylates using a photobase generator (PBG). The fabrication of dynamic polythioether ionogels based on this reaction was then demonstrated by loading 1-ethyl-3-methylimidazolium bis(trifluoromethylsulfonyl) imide (EMIM TFSI) or 1-ethyl-3-methylimidazolium trifluoromethanesulfonate (EMIM Triflate). They were chosen as ionic liquid in these ionogels owing to their high ionic conductivity. Thermal properties, mechanical properties, and the ionically conducting behavior of these ionogels were studied. Dynamic properties of these materials were examined with healing and stress relaxation experiments. To the best of our knowledge, these are the first vitrimer ionogels based on *S*-transalkylation exchange reaction. The design concept illustrated in this work could potentially open a new path for the development of flexible electrochemical-based electronics with a longer lifetime.

Experimental section

Materials

The photobase generator (PBG) 2-(9-oxoxanthen-2-yl)propionic acid 1,5,7-triazabicyclo[4.4.0]dec-5-ene salt and 1,4-butanediol bis(thioglycolate) (dithiol, DT) were purchased from TCI Chemicals. Poly(ethylene glycol) diacrylate (PEGDA, $M_n = 700$ g mol^{-1}), trimethylolpropane tris(3-mercoptopropianate) (trithiol, TT), triethylamine, 1-ethyl-3-methylimidazolium trifluoromethanesulfonate (EMIM Triflate), and sodium bicarbonate ($NaHCO_3$) were purchased from Sigma–Aldrich. 4-Bromobenzenesulfonyl chloride was purchased from Alfa Aesar. Magnesium sulfate heptahydrate ($MgSO_4 \cdot 7H_2O$) was obtained from Acros Organics. 1-Ethyl-3-methylimidazolium bis(trifluoromethylsulfonyl)imide (EMIM TFSI) was purchased from Solvionic. Finally, hydrochloric acid 37% (HCl) and dichloromethane (DCM) were obtained from VMR Chemicals.

Synthetic procedures

Synthesis of alkylation agent butyl-4-bromobenzenesulfonate (BuOBrs). The synthesis of the alkylation agent butyl-4-bromobenzenesulfonate (BuOBrs) (Fig. S1†) is adapted from the work of Hendriks *et al.*[24] In a round-bottom flask, 4-bromobenzenesulfonyl chloride (4 g, 15.65 mmol) is dissolved in 20 mL of dry dichloromethane (DCM) and the system is cooled at 0 °C. Next, a solution of 1-butanol (4.64 g,

62.6 mmol) and triethylamine (12.68 g, 125.2 mmol) in 20 mL dry DCM is added dropwise. The ice water bath is removed and the mixture is stirred at room temperature overnight. The reaction mixture is washed with water (100 mL), HCl (3 M, 100 mL), saturated $NaHCO_3$ (100 mL), and water (100 mL). $MgSO_4$ is added into the organic phase collected and then filtered. Finally, the solvent is evaporated under reduced pressure and the desired product is obtained. The successful synthesis of BuOBrs is confirmed by ^{1}H-NMR (Fig. S1†). ^{1}H NMR (400 MHz, $CDCl_3$) δ 7.84–7.58 (m, 4H), 4.06 (t, $J = 6.5$ Hz, 2H), 1.72–1.51 (m, 2H), 1.34 (h, $J = 7.7$, 7.0 Hz, 2H), 0.87 (t, $J = 7.4$ Hz, 3H).

Preparation of PTE-BuOBrs polythioether vitrimer networks. The alkylation agent (BuOBrs, 1,2 or 5 mol% to acrylate functional groups) is added into a vial containing PTE single network precursors stoichiometric mixture consisting of DT (0.2502 g, 1.05 mmol), TT (0.279 g, 0.7 mmol), PEGDA (1.47 g, 2.1 mmol) and 2.205 g acetone as the solvent ($m_{solvent} = 1.5 \times m_{PEGDA}$). In parallel, the photobase generator PBG (0.02 g, 0.049 mmol, 1 wt% of the total weight of thiol and acrylate precursors) is dissolved in 400 μL EtOH (50 mg mL^{-1}) and then added into the vial under a light-protected condition. The mixture is cast into a mold consisting of two glass plates separated by a 0.5 mm thick Teflon spacer. Free-standing PTE-BuOBrs films are obtained by curing the precursor solution with a UV curing conveyor system (Primarc UV Technology, Minicure, Mercury vapor Lamp, UV intensity 100 W cm^{-2}, duration of each scan 4 s). 30 UV scans were applied for each sample. The acetone is evaporated under vacuum after the synthesis at 50 °C for 1 day. A thermal treatment at 140 °C for 1.5 h is applied to covalently incorporate the alkylation agent into the polythioether network.

Methods and techniques

Nuclear magnetic resonance spectroscopy (NMR). ^{1}H NMR spectra were recorded at 297 K on a Bruker AVANCE 400 spectrometer at 400 MHz and referenced to the residual solvent peaks (^{1}H, δ 7.26 ppm for $CDCl_3$).

Infrared spectroscopy (IR). Attenuated total reflection (ATR)-FT-IR spectroscopy was performed using a Tensor 27 (Bruker) FT-IR instrument equipped with an ATR accessory unit (resolution 4 cm^{-1}, 32 scans).

Extractable content. Soxhlet experiments were performed with a BUCHI SpeedExtractor E-914. The extractable content was determined by 3 cycles of extraction in DCM at 60 °C under 100 bar. Each cycle lasts about 15 min.

Rheology. Rheological measurements were performed with an Anton Paar Physica MCR 301 rheometer equipped with CTD 450 temperature control device and a plate–plate geometry (Gap 500 μm, diameter 25 mm, plate; polymerization system made from a lower glass plate coupled with a UV lamp 142 mW cm^{-2}). A 1% deformation was imposed at 1 Hz. Storage modulus (G') and loss modulus (G'') were recorded as a function of time. The solution of precursors of materials was put in the rheometer geometry and measurements begin immediately with UV exposure at 30 °C.

Thermogravimetric analysis (TGA). TGA experiments were performed in air on a Q50 model (TA Instruments) applying a heating rate of 10 °C min^{-1} to 600 °C.

Differential scanning calorimetry (DSC). Glass transitions of the materials were determined by DSC. Sequences of temperature ramps (heating, cooling jump, heating, cooling, heating) in the −80 to 180 °C range were performed at 20 °C min^{-1} ramping up and 5 °C min^{-1} cooling down using a TA Instruments Q1000 equipped with a liquid nitrogen cooling accessory and calibrated using sapphire and high purity indium metal. All samples were prepared in hermetically sealed pans (5–10 mg/sample) and were referenced to an empty pan. The reported T_g values are from the second heating cycle.

Tensile testing. Traction experiments were performed on a Dynamic Mechanical Analyzer instrument (TA, Q800) in tensile mode at room temperature. A strain rate of 20% min^{-1} to 500% was applied with an initial strain of 0.05% and a preload force of 0.01 N to obtain stress–strain curves.

Scanning electron microscopy (SEM). Samples were mounted directly on SEM stubs and imaged using a Field Emission Gun Scanning Electron Microscope (GeminiSEM300, Carl Zeiss) with an acceleration voltage of 20 keV under high vacuum.

Dynamic mechanical analysis (DMA). DMA experiments were conducted on the Q800 in tension mode. Heating ramps were performed from −70 °C to 200 °C at a constant rate of 3 °C min^{-1} with a maximum strain amplitude of 0.05% at a fixed frequency of 1 Hz, and a preload force of 0.01 N.

Stress relaxation measurement. Stress relaxation measurements were carried out on the Q800 at different temperatures. A preload force of 0.01 N and a constant strain of 3% were applied and the stress decay was monitored over time.

Ionic conductivity. The ionic conductivity was measured by electrochemical impedance spectroscopy using a VSP 150 potentiostat (Biologic SA). Samples were placed between two gold electrodes and placed in a thermostated cell under argon atmosphere. Experiments were carried out in a temperature range from 25 to 100 °C, in the frequency range from 2 MHz to 1 Hz with a rate of 6 points per decade and for an oscillation potential of 10 mV. The ionic conductivity σ (S cm^{-1}) is calculated using the eqn (1):

$$\sigma = \frac{1}{Z}\frac{d}{S} \quad (1)$$

where Z is the real part of the complex impedance (ohms), d the thickness of the sample (cm), and S is the sample area (cm^2).

Healing test. The healing experiments were conducted in two different manners: stacked samples or edge-to-edge samples. Sample films were first cut into two pieces. Then the two pieces of the samples were either stacked together or closely placed in contact at their cross section in order to measure the ionic conductivity and mechanical properties of healed samples, respectively. The samples were protected by Teflon films and pressured by 2 glass plates with paper clips and then were heated at 140 °C for 2 h for PTE-BuOBrs films and 4 h for PTE-BuOBrs-IL ionogels in the oven.

Calculation of topology freezing temperature T_v and activation energy of the viscous flow E_a. Based on Maxwell's model for viscoelastic fluids, the stress relaxation behavior of the vitrimer can be described with eqn (2) where the relaxation time τ is

determined as the time required to relax to 37% ($1/e$) of initial stress:[25]

$$\frac{\sigma_{(t)}}{\sigma_0} = e^{-\frac{t}{\tau}} \quad (2)$$

For vitrimers, relaxation times reflect associative exchange reactions and their temperature dependence can be fitted to the Arrhenius equation (eqn (3)):[26,27]

$$\tau(T) = \tau_0 e^{\frac{E_a}{RT}} \quad (3)$$

The values of τ were then plotted as a function of temperature to determine the activation energy E_a of the viscous flow induced by the associative exchange reaction. The topology freezing temperature T_v is another key characteristic for vitrimer materials. Conventionally, the hypothetical T_v is chosen as the temperature at which the viscosity equals 10^{12} Pa s as this value describes the liquid-to-solid transition of a glass-forming liquid.[14,20] The relation between the viscosity η and the characteristic relaxation time τ can be expressed with the Maxwell relation (eqn (4)):[28]

$$\eta = G \times \tau = \frac{E'}{2(1+\nu)} \times \tau \quad (4)$$

where G stands for the shear modulus, ν for the Poisson's ratio and E' for the storage modulus at the rubbery plateau. Using the Poisson's ratio = 0.5 usually used for rubbers,[26,28] T_v is determined by combining eqn (3) and (4).

Results and discussion

Firstly, dynamic polythioether networks PTE-BuOBrs were prepared, *i.e.*, without ionic liquid, to investigate their different properties and to select the optimal alkylating agent content for the future dynamic ionogels. Our group have reported the preparation and characterization of PTE-based ionogels using photocatalyzed thiol–ene Michael addition between a mixture of different thiol and acrylate functional groups.[2] The resulting soft and stretchable ionogels with high ionic conductivity were obtained from poly(ethylene glycol) diacrylate (PEGDA), 1,4-butanediol bis(thioglycolate) (dithiol, DT) as chain extender trimethylolpropane tris(3-mercoptopropianate) (trithiol, TT) as crosslinker in the presence of 50 wt% ionic liquid relative to the total mixture weight. Therefore, the same composition of ionogel was used as starting point for the preparation of PTE-based polymer network in this work. PTE vitrimer was first synthesized by introducing BuOBr acting as alkylation agent into the polymer network. Ionogel vitrimer was then obtained by the *in situ* synthesis in the presence of ionic liquid *i.e.*, EMITFSI or EMI OTf. The chemical structures of all chemicals, illustration of dynamic ionogels PTE-BuOBrs-IL are shown in Scheme 1.

Synthesis and characterization of PTE-BuOBrs polythioether vitrimer networks

The PTE-BuOBrs polythioether vitrimer networks were first synthesized with the introduction of different quantities of BuOBrs (1, 2, 5 mol% *vs.* acrylate functional groups) with thiol and acrylate precursors in the presence of 1 wt% PBG (*vs.* the total weight of precursor mixture). Free-standing PTE-BuOBrs films were obtained by photopolymerization. A thermal activation at 140 °C for 1.5 h is necessary to covalently incorporate the alkylation agent into the PTE network.[29] As a blank, a network without BuOBrs was prepared. The compositions and properties of all samples are illustrated in Table 1.

Rheological studies were carried out on PTE-BuOBrs5 (sample containing 5 mol% of alkylation agent) and its corresponding

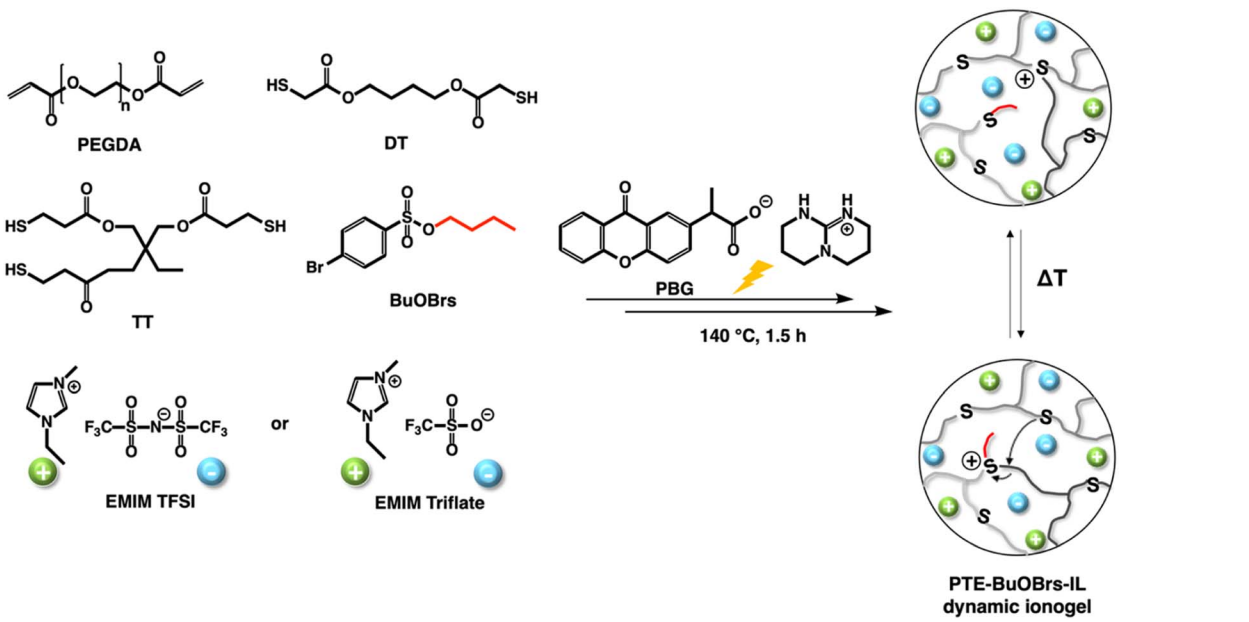

Scheme 1 Chemical structures of the chemicals and illustrations of polythioether vitrimer PTE-BuOBrs and dynamic ionogels PTE-BuOBrs-IL.

Table 1 Details of all PTE-BuOBrs samples and PTE control sample prepared with PEGDA, DT, and TT in a functional group molar ratio of 100 : 50 : 50 and various amounts of alkylation agent BuOBrs. Extractable contents of all samples before and after thermal treatment at 140 °C for 1.5 h are listed. Thermal and mechanical properties of thermal-treated PTE-BuOBrs networks and their reference PTE samples

Sample	BUOBRS (mol%)	Extractable content before thermal treatment (wt%)	Extractable content after thermal treatment (wt%)	T_g (DSC) (°C)	T_α (DMA) (°C)	Young's modulus (MPa)	Elongation at break (%)
PTE	0	3.9	3.6	−44.7	−30.0	1.7 ± 0.1	90 ± 11
PTE-BuOBrs1	1	7	3.8	−44.5	−25.6	1.3 ± 0.1	71 ± 19
PTE-BuOBrs2	2	6.7	7.7	−44.6	−24.3	1.2 ± 0.1	71 ± 1
PTE-BuOBrs5	5	7.7	14.3	−45.0	−21.0	1.1 ± 0.2	53 ± 20

control sample (PTE) by following the *in situ* photopolymerization of the precursor mixtures at 30 °C. Storage modulus (G') and loss modulus (G'') were recorded as a function of time (Fig. 1a). The initial viscosities of the PTE-BuOBrs5 and PTE precursor mixtures were low (about 0.1 Pa s), which enable possible coating applications. The gel points, where G' and G'' curves intersected, were reached in less than 20 s, indicating the fast polymerization kinetics of thiol–ene Michael addition under catalytic activation of the photobase. The two samples reached a similar G' plateau of about 300 kPa within 5 min. These results indicate the successful formation of polymer network through UV-activated thiol–ene Michael addition and that the presence of BuOBrs does not hinder the polymerization.

After verifying that the addition of alkylation agent does not disturb the formation of the polythioether networks, characterizations were carried out on PTE-BuOBrs samples that underwent a thermal activation at 140 °C for 1.5 h to covalently incorporate BuOBrs into the polymer network through alkylation of the thioether functions. The same procedure was also applied to the reference PTE sample. To verify the successful formation of polymer networks, soluble fractions of all UV-cured networks before and after thermal treatment were measured by Soxhlet extraction in DCM at 60 °C under 100 bar. Table 1 listed the soluble fractions of all materials. All samples except PTE-BuOBrs5 demonstrated similar and low extractable contents before and after the thermal treatment. This result indicates that the polymerization conditions are suitable for the formation of polymer network. To better understand the increase in soluble fraction of PTE-BuOBrs5 sample after thermal treatment, extractable contents of PTE and PTE-BuOBrs5 samples before and after thermal treatment were examined by ^{1}H NMR. The NMR spectrum of PTE before and

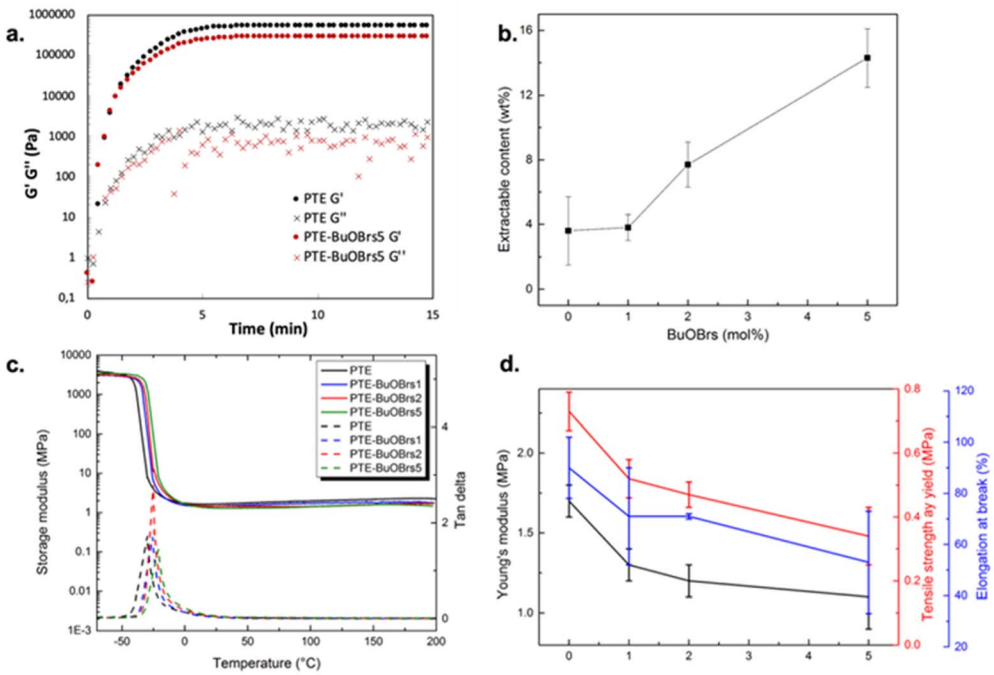

Fig. 1 (a) Rheological properties of PTE-BuOBrs5 and PTE precursor mixtures as a function of time during photopolymerization; (b) soluble fractions of PTE-BuOBrs samples after thermal treatment at 140 °C for 1.5 h as a function of alkylation agent content; (c) DMA curves of PTE-BuOBrs series samples and PTE control sample; (d) Young's modulus, tensile strength at yield and elongation at break extracted from the stress–strain test as a function of BuOBrs mol% of PTE-BuOBrs samples.

thermal treatment can be found in Fig. S2 and S3,† while those of PTE-BuOBrs5 before and thermal treatment can be found in Fig. S4 and S5.† The Soxhlet residues contained a large amount of oligo- or polythioether and traces of PEGDA, DT, and TT precursors. For PTE-BuOBrs5 sample, the alkylation agent could only be observed before thermal treatment, implying that the BuOBrs was successfully incorporated into the PTE networks after the thermal treatment. Concerning samples after applying thermal treatment of 1.5 h, an increase in soluble fractions has been observed with increasing alkylation agent content (Fig. 1b). This same tendency has been reported by Hendriks *et al.*,[24] which could probably be explained by the cleavage of network chain ends by exchange to a butyl group, thus being removed from the bulk material. Minimum amounts of acrylate bonds originating from PEGDA were only extracted from thermally treated PTE and PTE-BuOBrs5 samples. Integrations of peaks originating from precursors were examined and the ratio between PEGDA, DT, and TT was calculated. In the case of stoichiometric reactivity, the theoretical ratio of PEGDA/DT/TT extracted should be 6/3/2, as samples were prepared using PEGDA, DT and TT precursors with a functional group ratio of 100 : 50 : 50. Based on the calculation, residues of all samples after extraction were found to demonstrate ratios close to 6/3/2, which confirmed the stoichiometric reactivity of thiol Michael addition. Moreover, ratios of PEGDA, DT and TT extracted before and after the thermal treatment remained unchanged. These results indicate that despite the increase in sol fractions of PTE-BuOBrs5 sample, thermally treated PTE-BuOBrs and PTE networks still consisted of the same compositions as pristine samples.

After thermal treatment, PTE-BuOBrs sample should demonstrate an ionically conducting behavior thanks to the formation of alkyl sulfonium on the PTE network and 4-bromobenzenesulfonate counter-ion during the thermal activation, as depicted in Scheme 1. Thus, the ionically conducting behaviors of PTE-BuOBrs2 sample before and after thermal treatment have been studied. The non-treated material showed no conducting behavior, while the samples after thermal treatment demonstrated a low ionic conductivity of 1.8×10^{-7} S cm^{-1} at 60 °C. These results confirmed the presence of sulfonate counter-ions and consequently the successful alkylation of thioether groups through thermal treatment. After verifying the well-formed nature of PTE-BuOBrs and the incorporation of alkylation agent through thermal treatment, different characterizations were carried out on these materials.

Thermal and mechanical properties. Thermal and thermomechanical properties of crosslinked PTE-BuOBrs networks and the control sample PTE were investigated *via* differential scanning calorimetry (DSC) and dynamic mechanical analysis (DMA). Only activated PTE-BuOBrs and PTE samples were characterized. Thermograms of all materials are shown in Fig. S6.† All samples are completely amorphous, no crystallization nor melting could be observed. Moreover, these materials demonstrate only one glass transition, the onset T_g values of PTE-BuOBrs series samples are very similar, around −45 °C, and are listed in Table 1, indicating the similar nature and structure of the networks.

Fig. 1c shows the storage modulus and tan δ *versus* temperature of crosslinked PTE-BuOBrs networks with different loads of alkylation agent BuOBrs. At low temperatures, the storage modulus of glassy states of all samples were about 2 GPa, whereas the storage modulus decreased remarkably when the samples went through an evident and narrow α relaxation. All curves exhibit only one transition, which is in line with the results obtained by DSC. The onset temperature of the alpha transition slightly increased with the addition of BuOBrs. Furthermore, the storage moduli of rubbery states were similar. The relaxation temperature T_α of PTE-BuOBrs samples are resumed in Table 1. The slight increase in relaxation temperature with the BuOBrs load might be due to the increasing ionic interactions occurring after alkylation.

Tensile tests were performed on PTE-BuOBrs series samples to study the influence of alkylation agent content on the mechanical properties of the materials. Values of Young's modulus and elongation at break extracted from tensile tests are listed in Table 1 and are plotted as a function of BuOBrs content in Fig. 1d. It is clear that the modulus and stretchability of samples decrease with increasing alkylation agent content. This plasticizing-like effect can be explained by the presence of small uncrosslinked fractions evidenced by increasing extractable contents with BuOBrs content as well as the plasticizing role of 4-bromobenzenesulfonate.

Healing test. Vitrimers are polymers that can change their topology through dynamic exchange reactions without degenerating the network, maintaining a constant crosslink density.[14,20,26,30–32] At low temperatures, the topology of the network is frozen, and they behave like permanently cross-linked thermosets. At elevated temperatures, the network can flow by topology rearrangement and behave like viscoelastic liquids. To examine the dynamic nature of transalkylation exchange reaction, the healing abilities of PTE-BuOBrs series samples were studied by cutting film samples into two pieces and then stacking them together. The films were clipped between two glass plates at 140 °C for 2 h. These conditions were based on the stress relaxation tests (Fig. 3), one additional hour was set for ensuring that the viscous flow was possible with complete topology

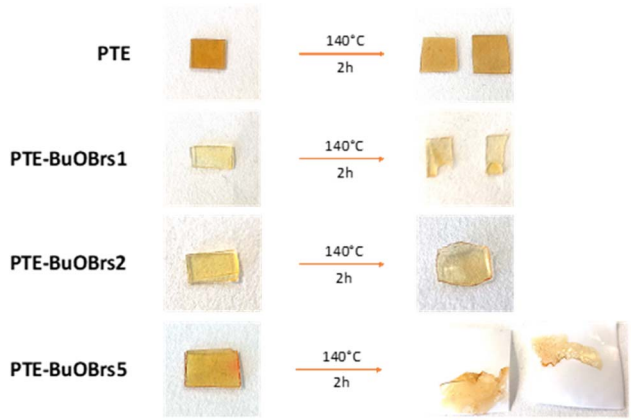

Fig. 2 Healing behavior of PTE-BuOBrs samples and PTE control sample at 140 °C during 2 h.

rearrangement. The healing test was also conducted with the single PTE control sample. Pictures of all samples before and after healing are shown in Fig. 2. After heating, films of PTE-BuOBrs2 and PTE-BuOBrs5 completely fused into one piece, no trace of the original films could be seen. In contrast, the PTE control sample films could be easily separated, no healing effect could be observed. These results proved that the transalkylation exchange reaction enabled by the alkylation agent is directly responsible for the healing behavior of our materials. However, despite that PTE-BuOBrs1 sample contained 1 mol% of alkylation agent, the two films could still be separated but with some difficulties. These results indicated that the content of 1 mol% of BuOBrs is insufficient for effective healing behavior. Thus, further characterizations will only be conducted on samples containing 2 and 5 mol% of BuOBrs.

Stress relaxation behaviour. Vitrimers are able to demonstrate macroscopic flow and to relax stress thanks to the dynamic exchange reactions at elevated temperature,[33] while conventional thermosets are resistant to relaxation under an applied strain due to their stable crosslinked networks.[34] To study the exchange dynamics of transalkylation reaction, PTE-BuOBrs2 and PTE-BuOBrs5 samples were subjected to stress relaxation experiments at various temperatures by monitoring the decrease of stress over time at a constant strain of 3%. The same tests were conducted on the PTE control sample without alkylation agent.

Fig. 3a compares the relaxation curves of samples containing 0, 2 and 5 mol% of alkylation agent at 140 °C, where the relative stress percentage is plotted as a function of time. Both PTE-BuOBrs2 and PTE-BuOBrs5 completely relaxed the applied stress after 86 min and 15 min respectively, whereas limited viscoelastic relaxation could be observed with the PTE control sample. These results provide convincing evidence that the alkylation agent BuOBrs plays a key role in network rearrangement in PTE-BuOBrs samples. Moreover, the full stress relaxation also indicates a swift exchange of thioether and sulfonium linkages and implies the dynamic nature of PTE-BuOBrs samples. Fig. 3b and c compare the stress relaxation behavior of PTE-BuOBrs2 and PTE-BuOBrs5 samples at different temperatures respectively. At 30 °C, after applying a constant deformation of 3% for 1 h, no significant stress relaxation could be seen in both samples. This result indicates that at low temperature, the transalkylation exchange reaction is inactivated and the network rearrangement is 'frozen', consequently these vitrimer materials behave like a classical crosslinked material. On the other hand, the relaxation rate increases with temperature, proving the temperature-dependent nature of the dynamic exchange reaction.

Relaxation time is defined as the time required to relax to 37% ($1/e$ according to the Maxwell model for viscoelastic fluids) of initial stress.[25] By comparing the stress relaxations curves shown in Fig. 3b and c, PTE-BuOBrs samples with higher BuOBrs content exhibit a lower relaxation time at the same temperature. Indeed, a faster network reorganization is expected with an increasing number of associative exchangeable bonds. One important feature of vitrimers is that they

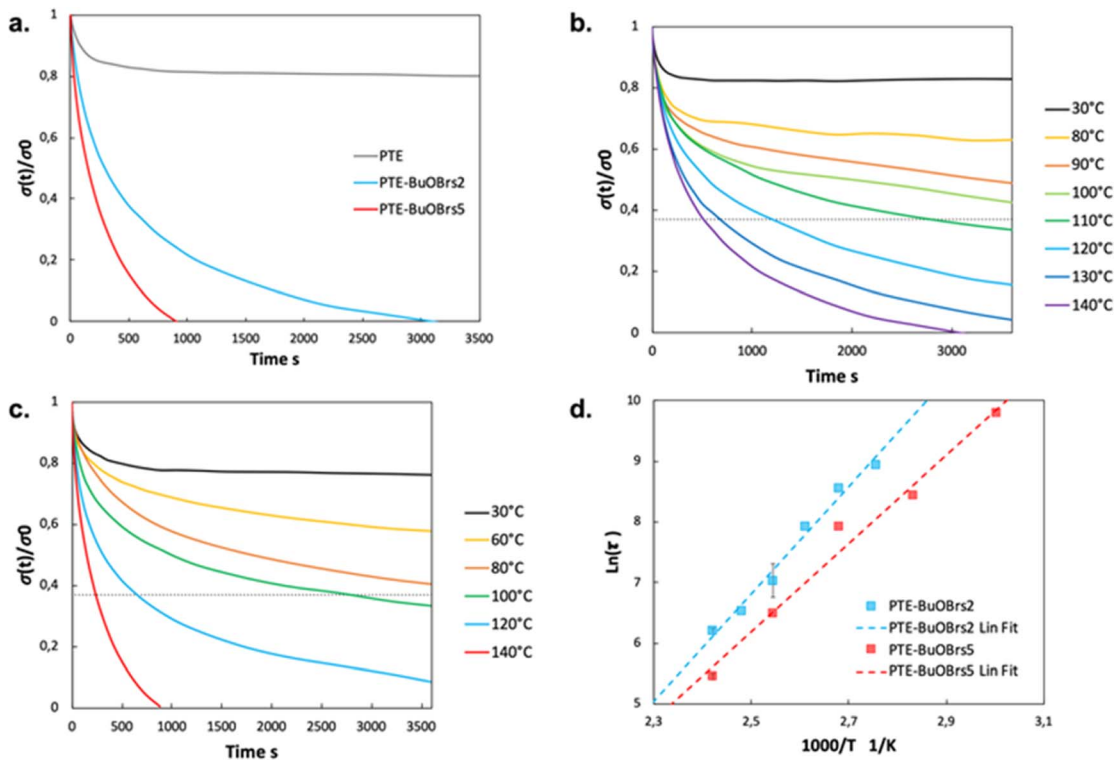

Fig. 3 (a) Stress relaxation behaviors of PTE-BuOBrs samples with 2 and 5 mol% of alkylation agent content and their control sample PTE at 140 °C; (b) stress relaxation curves of PTE-BuOBrs2 sample at different temperatures (c) stress relaxation curves of PTE-BuOBrs5 sample at different temperatures; (d) Arrhenius linear fit of relaxation times of PTE-BuOBrs2 and PTE-BuOBrs5 samples plotted as a function of 1000/T.

Table 2 Relaxation times extracted from stress relaxation tests of PTE-BuOBrs samples and their corresponding theoretical T_v and E_a associated with the transalkylation exchange reaction extracted from stress relaxation tests of PTE-BuOBrs samples

Sample	T_V (°C)	E_a (kJ mol^{-1})
PTE-BuOBrs2	23	73.6
PTE-BuOBrs5	1	60.6

demonstrate an Arrhenius-like gradual decrease of viscosity at higher temperatures. To confirm the associative exchange mechanism of transalkylation reaction, relaxation times were plotted as a function of temperature. As shown in Fig. 3d, the relaxation times indeed followed the Arrhenius law, and an activation energy of 73.6 kJ mol^{-1} and 60.6 kJ mol^{-1} were calculated from the slope of Arrhenius linear fit of PTE-BuOBrs2 and PTE-BuOBrs5, respectively. These values are lower than those reported in the litterature,[29,35,36] probably because of the polar environment of our polymer matrix which favors the transalkylation reaction that takes place between ionic reactants. The more available alkyl sulfonium existing in PTE-BuOBrs5 network resulted in faster exchange kinetics and consequently lower activation energies of the viscous flow. The topology freezing temperature T_v is another characteristic for vitrimer materials. T_v values were extrapolated based on the method described in the experimental section (Table 2). The hypothetical T_v of PTE-BuOBrs2 and PTE-BuOBrs5 samples were calculated to be 23 °C and 1 °C respectively. These values of T_v seems to indicate that the transalkylation reaction can start to take place at a such low temperature, while stress-relaxation experiments state a behavior similar to that of PTE network. Indeed, Du Prez *et al.* pointed out that extrapolation could result in significant errors when determining T_v in low T_g vitrimer materials,[37] as in our case. The hypothetical T_v can be considered more as an estimation of relative importance for the exchange mechanism than a crucial characteristic of the materials. The fact that T_v value decreases with the increase in BuOBrs content is in line with the increase in dynamic site for exchange reaction, leading to a faster achievement of liquid-to-solid transition.

Synthesis and characterization of polythioether vitrimer ionogel – PTE-BuOBrs-IL. PTE-BuOBrs materials demonstrated vitrimer properties such as healing and stress relaxation thanks to the dynamic transalkylation exchange reaction enabled by the alkylation agent. For efficient vitrimer effect through thioether linkages, at least 2 mol% of BuOBrs (*vs.* theoretical content of thioether groups) need to be added into the polythioether networks. To combine these interesting vitrimer properties with ionic conducting behavior, ionic liquids were incorporated into these networks. A content of 2 mol% of BuOBrs was selected because it gives a vitrimer network with an interesting working temperature range, *i.e.*, the network keeps mechanical integrity up to 80 °C, and with an adequate reprocessing window through efficient vitrimer effect above 80 °C. 50 wt% of either EMIM TFSI or EMIM triflate compared to the total weight was introduced into the precursor mixture and the formation of ionogel was achieved *in situ*. Illustration of the PTE-BuOBrs-IL dynamic ionogel is shown in Scheme 1. Table 3 compares properties of PTE-BuOBrs-IL ionogels with PTE-BuOBrs2 samples and characterizations were carried out on ionogel samples after thermal treatment.

The rheological properties of the PTE-BuOBrs2-TFSI50 and PTE-BuOBrs2-Trif50 precursor mixtures were monitored during photopolymerization (Fig. S7†). The initial viscosities of the two precursor mixtures were 0.17 and 0.11 Pa s, respectively. Gel points were reached within 20 s. A G' plateau of about 250 kPa and a G'' plateau of 680 Pa were reached within 5 min, demonstrating similar polymerization kinetics to PTE-BuOBrs samples. Soluble fractions of PTE-BuOBrs2-TFSI50 and PTE-BuOBrs2-Trif50 in DCM were 47.8% and 49.2% respectively. Bearing in mind that 50 wt% of ILs were incorporated into ionogels, these results demonstrated the well-formed nature of the polymer networks.

Thermal and mechanical properties of the ionogels. Thermal properties of crosslinked PTE-BuOBrs2-TFSI50 and PTE-BuOBrS2-Trif50 samples were studied and compared with PTE-BuOBrs2. All samples are completely amorphous materials as they display only one glass transition (Fig. S8†). T_g values of −51.2 °C and −55.8 °C were measured for PTE-BuBrs2-TFSI50 and PTE-BuOBrs2-Trif50, respectively. They are lower than that of PTE-BuOBrs2 (T_g = −44.6 °C) because of a plasticizing effect induced by ILs. This trend is also observed by DMA for all samples, with slightly lower storage modulus at both glassy and rubbery states and lower T_α values (Fig. 4a). Tensile tests were conducted on PTE-BuOBrs2-TFSI50 and PTE-BuOBrs2-Trif50 samples. Values of Young's modulus and elongation at break extracted from tensile tests are listed in Table 3. The addition of ILs decreased the tensile strength of the polymer networks and led to less extensible materials.

Ionic conductivity behavior of ionogels. The ionic conductivity behaviors of PTE-BuOBrs-IL ionogels at different temperatures were studied by electrochemical impedance spectroscopy (Fig. 4b). At 25 °C, PTE-BuOBrs2-TFSI50 and PTE-BuOBrs2-Trif50 demonstrated high ionic conductivities of 2.8 × 10^{-4} S cm^{-1} and 3.2 × 10^{-4} S cm^{-1}, respectively. Such conductivity was shown to be able to satisfy a variety of flexible

Table 3 Compositions and details of PTE-BuOBrs-IL samples

Sample	IL type	IL content (wt%)	Extractable content after TC (wt%)	T_g (DSC) (°C)	T_α (DMA) (°C)	Young's modulus (MPa)	Elongation at break (%)
PTE-BUOBRS2	—	—	7.7	−44.6	−24.3	1.2 ± 0.1	71 ± 1
PTE-BUOBRS2-TFSI50	EMIM TFSI	50	47.8	−51.2	−29.5	0.9 ± 0	55 ± 1
PTE-BUOBRS2-Trif50	EMIM triflate	50	49.2	−55.8	−29.5	0.9 ± 0.1	33 ± 13

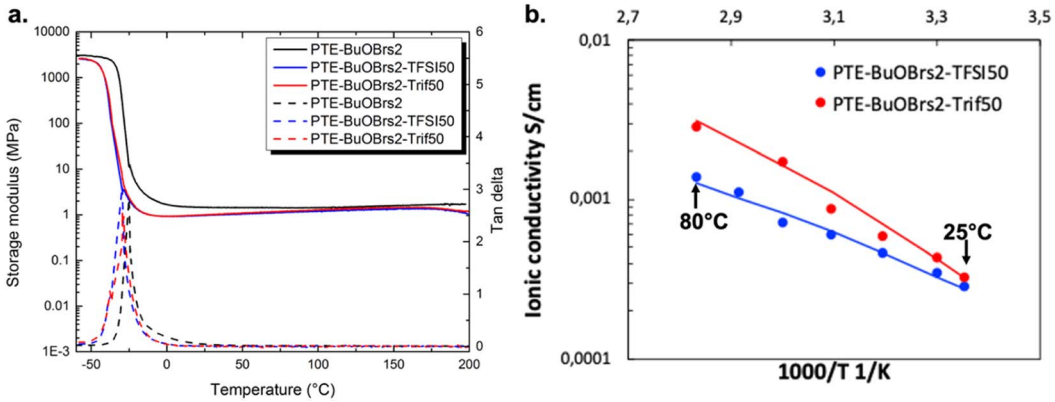

Fig. 4 (a) DMA tests of PTE-BuOBrs-IL ionogels and PTE-BuOBrs2 sample; (b) ionic conductivity of PTE-BuOBrs2-TFSI50 and PTE-BuOBrs2-Trif50 samples at different temperatures. Solid lines: calculation according to VTF equation.

Table 4 Ionic conductivity behavior of PTE-BuOBrs2-TFSI50 and PTE-BuOBrs2-Trif50

Sample	T_g (°C)	Ionic conductivity at 30 °C (S cm^{-1})	A (VTF) (S K$^{1/2}$·cm^{-1})	E_a (VTF) (kJ mol^{-1})	R^2 (VTF)
PTE-BuOBrs2-TFSI50	−51.2	2.8×10^{-4}	1.0	5.6	0.9838
PTE-BuOBrs2-Trif50	−55.8	3.2×10^{-4}	12.4	8.5	0.9818

electronic applications, such as ionic conductor in sensors and solid electrolytes in electroactive devices.[13] By increasing the temperature, the ionic conductivities increased as the ion mobility rises to finally reach 1.4×10^{-3} S cm^{-1} and 2.9×10^{-3} S cm^{-1} at 80 °C respectively. The temperature dependence of these polymer electrolytes can be described by the Vogel–Tamman–Fulcher (VTF) equation:

$$\sigma = AT^{-\frac{1}{2}}e^{-\frac{E_a}{R(T-T_0)}}$$

where A is a temperature-independent constant related to the number of charge carriers, E_a is the pseudo-activation energy related to polymer segmental motion and R stands for the gas constant. T_0 is a reference temperature usually correlated with the ideal glass transition temperature at which free volume disappears or at which the configurational entropy of the polymer chain becomes zero. T_0 is usually 35 to 50 K below T_g in either case.[38–40] The VTF behaviors of all PTE-BuOBrs-IL samples were studied with T_0 set to T_g – 50 K and all parameters extrapolated are listed in Table 4. The values of R^2 of the VTF linear fit are about 0.99, which shows that the VTF model is suitable for describing the ionic behavior of these materials, indicating that the movements of the charge carrier are correlated with the polymer chain movements. The parameter A was found to be 1.0 S K$^{1/2}$ cm^{-1} for PTE-BuOBrs2-TFSI50 sample and 12.4 S K$^{1/2}$ cm^{-1} for PTE-BuOBrs2-Trif50, while the E_a of ionic conduction of 5.6 kJ mol^{-1} and 8.5 kJ mol^{-1} was assigned to each material. The higher A parameter which is correlated to the number of charge carriers can be explained by the higher cation

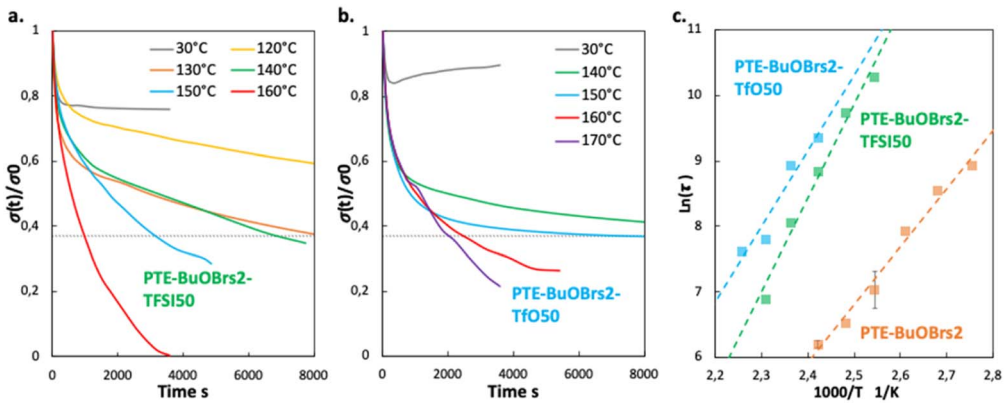

Fig. 5 (a) Stress relaxation tests of PTE-BuOBrs2-TFSI50 sample at various temperatures; (b) stress relaxation tests of PTE-BuOBrs2-Trif50 sample at various temperatures; (c) Arrhenius linear plot extracted from relaxation times of PTE-BuOBrs2-TFSI50, PTE-BuOBrs2-TFSI50 and PTE-BuOBrs2 samples at different temperatures.

and anion concentration of EMIM triflate (5.3 mol L^{-1}) than EMIM TFSI (3.9 mol L^{-1}).[41] Moreover, compared to the hydrophobic EMIM TFSI, EMIM triflate is known to be more hydrophilic,[42] thus more susceptible to absorb ambient humidity, resulting in a higher conductivity in open air condition with better ion dissociation.

Dynamic behavior of the ionogels. PTE-BuOBrs2 sample has exhibited vitrimer properties such as healing and stress relaxation. PTE-BuOBrs-IL ionogels were also subjected to the same experiments to check if the presence of ILs within the material would modify their vitrimer properties. Stress relaxation curves of PTE-BuOBrs2-TFSI50 and PTE-BuOBrs2-Trif50 samples are shown in Fig. 5a and b, respectively. At 30 °C, slight stress relaxation followed by a stress plateau can be seen in both samples as the transalkylation exchange reaction and the corresponding network rearrangement is not occurring significantly at this temperature. On the whole, the ionogels relax at higher temperatures than the PTE-BuOBrs samples, *i.e.*, above 120 °C. For instance, at 140 °C a relaxation time of 114.8 min was observed for PTE-BuOBrs2-TFSI50 and 190.8 min for PTE-

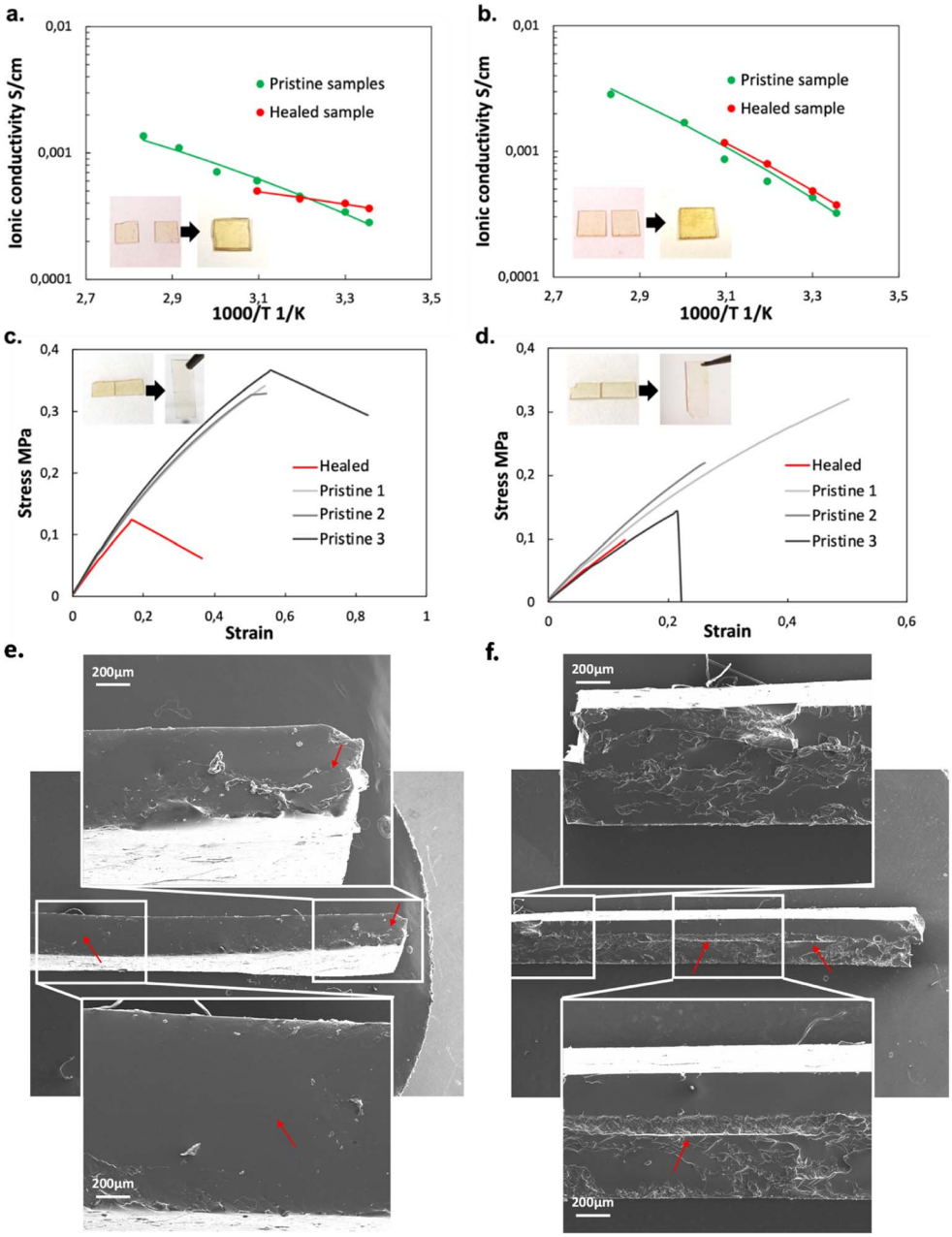

Fig. 6 (a) Pictures and the ionic conductivity behavior of PTE-BuOBrs2-TFSI50 before and after stacked healing; (b) pictures and the ionic conductivity behavior of PTE-BuOBrs2-Trif50 before and after stacked healing; (c) pictures and the tensile testing curves of PTE-BuOBrs2-TFSI50 before and after interfacial healing; (d) pictures and the tensile testing curves of PTE-BuOBrs2-Trif50 before and after interfacial healing; SEM image of the cross-section of two pieces of (e) PTE-BuOBrs2-TFSI50 after stacked healing and of (f) PTE-BuOBrs2-Trif50 after stacked healing.

BuOBrs2-Trif50, which were much higher than that of PTE-BuOBrs2 sample (relaxation time 8.2 min). This significant decrease of relaxation rate after adding ILs could be possibly explained by a dilution effect of the dynamic alkyl sulfonium/thioether bonds by the IL but also by a screening effect of the ions from the IL on the sulfonium/$OBrs^-$ couple. We further studied the stress relaxation behavior of these ionogels at higher temperatures. For both PTE-BuOBrs2-TFSI50 and PTE-BuOBrs2-Trif50, the relaxation rates increased with increasing temperature. PTE-BuOBrs2-TFSI50 sample relaxed stress fully after 1 h at 160 °C and PTE-BuOBrs2-Trif50 sample relaxed 80% of the stress after 1 h at 170 °C. Fitting the relaxation times to the Arrhenius equation (Fig. 5c) gives a calculated transalkylation exchange reaction E_a of 119.0 kJ mol^{-1} for PTE-BuOBrs2-TFSI50 and 96.0 kJ mol^{-1} for PTE-BuOBrs2-Trif50, which are higher than that of PTE-BuOBrs2 (73.6 kJ mol^{-1}). This higher activation energies are due probably to the modification of the polarity environment in the presence of IL. On the other hand, the hypothetical T_v increased to around 79 °C and 74 °C for the two materials in the presence of IL. These results are in accordance with the observed longer relaxation times and slower exchange rates. It indicates that higher energy is required to realize network rearrangement of these dynamic ionogels but also that the ionogel topology is stable over a larger temperature range than its PTE network counterpart, which can be promising for application into practical devices.

Healability of the ionogels. PTE-BuOBrs-IL samples have demonstrated Arrhenius-like temperature dependency of relaxation times at elevated temperatures. These materials are also expected to display healing properties because of the dynamic transalkylation exchange of alkyl sulfonium ions. The dynamic ionogels were subjected to two different healing experiments at 140 °C for 4 h (well above the relaxion time at 140 °C) where two pieces of the samples were either stacked together or laterally assembled edge-to-edge. For healable ionogels, the materials must retrieve both their ionically conducting behavior and mechanical properties after failure. Thus, ionic conductivity measurements have been carried out for face-to-face stacked samples after the healing experiment, while tensile testings have been performed for samples after edge-to-edge healing.

Pictures of PTE-BuOBrs2-TFSI50 and PTE-BuOBrs2-Trif50 samples before and after stacked healing tests can be found in Fig. 6a and b respectively. For both samples, the two films couldn't be separated after the healing process, demonstrating that co-bonding took place at the interface thanks to the dynamic bond exchanges. However, the two pieces are not fused together as it was observed for the PTE-BuOBrs2 without IL, demonstrating either a lower healing efficiency or incomplete healing due to the much slower dynamic kinetics. These observations are consistent with the results obtained from stress relaxation experiments, which is the addition of ILs results in slower network rearrangement. The stacked healed samples showed similar ionically conducting behaviors as pristine samples (Fig. 6a and b), indicating that the healing process was able to ensure the ionic conduction between the two films and recover the pristine ionic conducting behavior. Fig. 6c and d present tensile test experiments as well as pictures of PTE-BuOBrs2-TFSI50 and PTE-BuOBrs2-Trif50 films after the edge-to-edge healing test respectively. After 4 h at 140 °C, the fractured surfaces fused together, and the cracks were almost invisible to the eye. Tensile testing of the two samples showed that the healed samples demonstrated very similar Young's modulus as pristine samples (about 0.8 MPa), indicating that the topological rearrangement enabled by transalkylation seems to have retrieved the pristine mechanical properties within the elastic domain. The elongation at break reduced sharply (down to 55%) with breaks localized randomly and not especially on the healing area. Healing conditions of 4 h at 140 °C allowed fractured samples to weld together but it seems that long time exposure to high temperature reduced the elasticity of the materials. After healing, scares are not visible with the eyes but residual traces of it can be guessed on the image of the cross-section of stacked healed ionogels, especially on the EMIM Triflate based one (red arrows in Fig. 6e and f).

Conclusions

In this work, PTE-BuOBrs vitrimers were synthesized through the thiol–ene Michael addition between multifunctional thiol and diacrylate using a photobase generator. These PTE-BuOBrs networks exhibited vitrimer properties after thermal activation treatment, allowing the formation of alkylsulfonium salts. Healing and stress relaxation at elevated temperatures were demonstrated thanks to the *S*-transalkylation exchange reaction of sulfonium salts with thioether nucleophiles. These materials could completely relax stress and demonstrated viscous flow energies ranging from 60.6 kJ mol^{-1} and 73.6 kJ mol^{-1}. Vitrimer ionogels were then developed by synthesizing the PTE network in the presence of EMIM TFSI or EMIM triflate. These ionogels demonstrated Young's modulus of 0.9 MPa and ionic conductivities in the order of 10^{-4} S cm^{-1} at room temperature. Dynamic properties of these materials were examined with healing and stress relaxation experiments. It has been found that the addition of ILs modify the dynamic properties of the systems, probably because of a dilution effect of the dynamic functions by the IL but also because of a screening effect of the alkyl sulfonium $OBrs^-$ couple by the ions of the IL itself. A slowing down of the dynamic exchange kinetics and an increase of both their activation energy and T_v is observed. While it is resulting in a less efficient dynamic healing at a given temperature, it can provide also more dimensionally stable networks at application temperatures. To the best of our knowledge, this is the first work reporting vitrimer ionogels based on *S*-transalkylation exchange reaction. The ionogels developed herein are using mostly commercially available products, thus providing a simple and effective approach to developed tunable dynamic ionogels for flexible electronics with a longer lifespan.

Abbreviations

PEGDA	Poly(ethylene glycol) diacrylate
DT	1,4-Butanediol bis(thioglycolate)
TT	Trimethylolpropane tris(3-mercoptopropianate)

PBG	2-(9-Oxoxanthen-2-yl)propionic acid 1,5,7-triazabicyclo[4.4.0]dec-5-ene salt
IL	Ionic liquid
PTE	Polythioether
BuOBrs	Alkylating agent
EMIM TFSI	1-Ethyl-3-methylimidazolium bis(trifluoromethylsulfonyl)imide
EMIM Triflate	1-Ethyl-3-methylimidazolium trifluoromethanesulfonate

Author contributions

The manuscript was written through contributions of all authors. All authors have given approval to the final version of the manuscript.

Conflicts of interest

There are no conflicts to declare.

Acknowledgements

This project has received funding from the European Union's Horizon 2020 Research and Innovation Program under grant agreement No. 825232 "WEAFING".

References

1 Y. Zhong, G. T. M. Nguyen, C. Plesse, F. Vidal and E. W. H. Jager, *ACS Appl. Mater. Interfaces*, 2018, **10**, 21601–21611.
2 Y. Zhong, G. T. M. Nguyen, C. Plesse, F. Vidal and E. W. H. Jager, *J. Mater. Chem. C*, 2019, **7**, 256–266.
3 C. H. Yang, B. Chen, J. J. Lu, J. H. Yang, J. Zhou, Y. M. Chen and Z. Suo, *Extreme Mech. Lett.*, 2015, **3**, 59–65.
4 G. Gu, H. Xu, S. Peng, L. Li, S. Chen, T. Lu and X. Guo, *Soft Robot.*, 2019, **6**, 368–376.
5 Z. Deng, H. Wang, P. X. Ma and B. Guo, *Nanoscale*, 2020, 1224–1246.
6 C. Yang and Z. Suo, *Nat. Rev. Mater.*, 2018, **3**, 125–142.
7 Y. Ren, J. Guo, Z. Liu, Z. Sun, Y. Wu, L. Liu and F. Yan, *Sci. Adv.*, 2019, **5**, eaax0648.
8 J. Le Bideau, L. Viau and A. Vioux, *Chem. Soc. Rev.*, 2011, **40**, 907–925.
9 E. Andrzejewska, A. Marcinkowska and A. Zgrzeba, *Polymers*, 2017, **62**, 344–352.
10 S. Xiang, F. Zheng, S. Chen and Q. Lu, *ACS Appl. Mater. Interfaces*, 2021, **13**, 20653–20661.
11 D. Weng, F. Xu, X. Li, S. Li, Y. Li and J. Sun, *ACS Appl. Mater. Interfaces*, 2020, **12**, 57477–57485.
12 Y. Shi, Y. Wang, Y. Gu, L. Zheng, S. Ma and X. Xu, *Chem. Eng. J.*, 2020, **392**, 123645.
13 X. Qu, W. Niu, R. Wang, Z. Li, Y. Guo, X. Liu and J. Sun, *Mater. Horizons*, 2020, **7**, 2994–3004.
14 W. Denissen, J. M. Winne and F. E. Du Prez, *Chem. Sci.*, 2016, **7**, 30–38.
15 A. M. Wemyss, C. Bowen, C. Plesse, C. Vancaeyzeele, G. T. M. Nguyen, F. Vidal and C. Wan, *Mater. Sci. Eng., R*, 2020, **141**, 100561.
16 N. J. Van Zee and R. Nicolaÿ, *Prog. Polym. Sci.*, 2020, **104**, 101233.
17 Z. Tang, X. Lyu, A. Xiao, Z. Shen and X. Fan, *Chem. Mater.*, 2018, **30**, 7752–7759.
18 T. Li, Y. Wang, S. Li, X. Liu and J. Sun, *Adv. Mater.*, 2020, **32**, 2002706.
19 J. M. Winne, L. Leibler and F. E. Du Prez, *Polym. Chem.*, 2019, **10**, 6091–6108.
20 D. Montarnal, M. Capelot, F. Tournilhac and L. Leibler, *Science*, 2011, **334**, 965–968.
21 J. Liu, H. Song, Z. Wang, J. Zhang, J. Zhang and X. Ba, *J. Mater. Sci.*, 2020, **55**, 3991–4004.
22 J. Xu, H. Wang, X. Du, X. Cheng, Z. Du and H. Wang, *Chem. Eng. J.*, 2021, **426**, 130724.
23 J. Tang, J. Yang, H. Yang, R. Miao, R. Wen, K. Liu, J. Peng and Y. Fang, *J. Mater. Chem. C*, 2018, **6**, 12493.
24 Q. L. Lei, X. Xia, J. Yang, M. P. Ciamarra, R. Ni, M. Pica Ciamarra and R. Ni, *Proc. Natl. Acad. Sci. U. S. A.*, 2020, **117**, 27111–27115.
25 T. Wright, T. Tomkovic, S. G. Hatzikiriakos and M. O. Wolf, *Macromolecules*, 2019, **52**, 36–42.
26 W. Denissen, G. Rivero, R. Nicolaÿ, L. Leibler, J. M. Winne and F. E. Du Prez, *Adv. Funct. Mater.*, 2015, **25**, 2451–2457.
27 Y. Yang, S. Zhang, X. Zhang, L. Gao, Y. Wei and Y. Ji, *Nat. Commun.*, 2019, **10**, 1–8.
28 C. He, S. Shi, D. Wang, B. A. Helms and T. P. Russell, *J. Am. Chem. Soc.*, 2019, **141**, 13753–13757.
29 B. Hendriks, J. Waelkens, J. M. Winne and F. E. Du Prez, *ACS Macro Lett.*, 2017, **6**, 930–934.
30 M. Röttger, T. Domenech, R. Van Der Weegen, A. Breuillac, R. Nicolaÿ and L. Leibler, *Science*, 2017, **356**, 62–65.
31 A. Breuillac, A. Kassalias and R. Nicolaÿ, *Macromolecules*, 2019, **52**, 7102–7113.
32 D. J. Fortman, J. P. Brutman, G. X. De Hoe, R. L. Snyder, W. R. Dichtel and M. A. Hillmyer, *ACS Sustain. Chem. Eng.*, 2018, **6**, 11145–11159.
33 M. Chen, L. Zhou, Y. Wu, X. Zhao and Y. Zhang, *ACS Macro Lett.*, 2019, **8**, 255–260.
34 J. Han, T. Liu, C. Hao, S. Zhang, B. Guo and J. Zhang, *Macromolecules*, 2018, **51**, 6789–6799.
35 Z. Tang, Y. Liu, Q. Huang, J. Zhao, B. Guo and L. Zhang, *Green Chem.*, 2018, **20**, 5454–5458.
36 W. Xu, W. Yu, X. Chen, S. Liao and M. Luo, *J. Appl. Polym. Sci.*, 2021, 51182.
37 M. Guerre, C. Taplan, J. M. Winne and F. E. Du Prez, *Chem. Sci.*, 2020, **11**, 4855–4870.
38 G. Adam and J. H. Gibbs, *J. Chem. Phys.*, 1965, **43**, 139–146.
39 C. A. Angell, *Solid State Ionics*, 1983, **10**, 3–16.
40 M. C. Wintersgill and J. J. Fontanella, *Polymer Electrolyte Reviews*, Elsevier, London and New York, 1989, vol. 2.
41 P. Bonhôte, A.-P. Dias, N. Papageorgiou, K. Kalyanasundaram and M. Grätzel, *Inorg. Chem.*, 1996, **35**, 1168–1178.
42 G. García-Miaja, J. Troncoso and L. Romaní, *J. Chem. Thermodyn.*, 2009, **41**, 161–166.